TDSSC: A Three-Directions Spectral–Spatial Convolution Neural Network for Hyperspectral Image Change Detection

Tianming Zhan, Bo Song, Le Sun, Xiuping Jia, *Senior Member, IEEE*, Minghua Wan, Guowei Yang, and Zebin Wu, *Senior Member, IEEE*

***Abstract*—Change detection (CD) is a hot issue in the research of remote sensing technology. Hyperspectral images (HSIs) greatly promote the development of CD technology because of their high resolution in the spectral domain. However, some traditional CD methods currently applied to low-dimensional and multispectral images cannot adapt to the complex high-dimensional features of the HSIs. In addition, the spectral measurements of the HSI contain a lot of noise and redundancy, which greatly contaminates spectral-only information for CD. In order to fully extract the discriminant features of HSI to improve the accuracy of CD, this article proposes a three-directions spectral–spatial convolution neural network (TDSSC). A novel method for three-direction decomposition of hyperspectral change tensors is proposed—change tensor is decomposed along the spectral direction and two spatial directions to get a single tensor containing the spectral information and two kinds of tensors containing the spectral–spatial information. TDSSC uses 1-D convolution to extract spectral features from the spectral direction as well as reducing the tensor dimension, which helps the latter network to be lightweight and significantly improves the speed of change detection. Also, it uses 2-D convolution to extract spectral–spatial features from two spatial directions of the reduced tensor, and to extract features from different directions to improve the accuracy and Kappa value of CD. The experimental results of three real hyperspectral datasets show that TDSSC is superior to most existing CD methods.**

***Index Terms*—Change detection (CD), hyperspectral image (HSI), spectral–spatial combination, three directions convolution neural network.**

Manuscript received October 3, 2020; revised October 21, 2020; accepted November 1, 2020. Date of publication November 10, 2020; date of current version January 6, 2021. This work was supported in part by the National Natural Science Foundation of China under Grant 61976117, Grant 61876213, and Grant 61772274, in part by the Natural Science Foundation of Jiangsu Province under Grant BK20191409 and Grant BK20180018, in part by the Key Projects of University Natural Science Fund of Jiangsu Province under Grant 19KJA360001 and Grant 18KJA520005, in part by the Fundamental Research Funds for the Central Universities, under Grant 30917015104, Grant 30919011103, and Grant 30919011402, in part by the Collaborative Innovation Center of Audit Information Engineering and Technology under Grant 18CICA09, in part by the Young Teacher Research and Cultivation Project of Nanjing Audit University under Grant 18QNPY015, and in part by the Postgraduate Research & Practice Innovation Program of Jiangsu Province under Grant KYCX20_1680. *(Corresponding author: Zebin Wu.)*

Tianming Zhan is with the Collaborative Innovation Center of Audit Information Engineering and Technology and the School of Information Engineering, Nanjing Audit University, Nanjing 211815, China (e-mail: ztm@nau.edu.cn).

Bo Song, Minghua Wan, and Guowei Yang are with the School of Information Engineering, Nanjing Audit University, Nanjing 211815, China (e-mail: mg1909003@stu.nau.edu.cn; wanmh@sina.com; ygw_ustb@163.com).

Le Sun is with the School of Computer and Software, Nanjing University of Information Science and Technology, Nanjing 210044, China (e-mail: sunlecncom@nuist.edu.cn).

Xiuping Jia is with the School of Engineering and Information Technology, The University of New South Wales, Canberra, BC 2610, Australia (e-mail: x.jia@adfa.edu.au).

Zebin Wu is with the Nanjing University of Science and Technology, Nanjing 210094, China (e-mail: zebin.wu@gmail.com).

Digital Object Identifier 10.1109/JSTARS.2020.3037070

I. Introduction

REMOTE sensing satellite hyperspectral image (HSI) is a dataset that contains spatial information and abundant spectral information. It has become an important data source for object observation because it contains more spectral information than multispectral images (MSI). Change detection (CD) using multiperiod remote sensing satellite image technology has important application value in land cover analysis [1], ecosystem monitoring [2], portraying urban change [3], and so forth. The task of remote sensing image CD includes the following—to judge whether changes have occurred, to determine where changes have occurred, and to identify the types of changes. These tasks and their combinations correspond to commonly used CD types for remote sensing images [4]—anomaly CD [5]–[9], binary CD [10]–[15], multiclass CD [16], [17], and time-series CD [18], [19].

The CD of remote sensing images can generally be divided into four steps [20]—data acquisition, data preprocessing, change detection, and results output. The algorithm of CD is the core of determining the CD result. In the problem of single-band and multispectral CD, many researchers have proposed a variety of detection algorithms, such as change vector analysis, principal component analysis, iterative multivariate change detection, and so on. The main starting point of these methods is to extract the characteristics of spectral change vectors by algebraic operation, image transformation, and statistical analysis. In low-dimensional space, these methods have achieved high accuracy. However, the MSI CD algorithm for low-dimensional space is not ideal for high-dimensional HSI CD tasks [21], [22]. In addition, due to the high resolution of HSI, the spectral information of the two adjacent bands is usually highly correlated [4], which inevitably results in data redundancy. Therefore, how to analyze and process HSI data and extract useful information from a large amount of redundant data has become an important topic in the study of HSI CD.

In order to solve the problem of high-dimensional space and the large amount of data redundancy, deep learning has become

an effective solution. Deep learning facilitates the processing of complex hyperspectral data by effectively extracting the abstract features of the data while reducing the dimensions of the data. The use of a convolution neural network makes it possible to use the spectral information of pixel points and their neighboring pixels in the process of CD, which largely avoids the limitation of using only the spectral information corresponding to a single pixel point. With in-depth research, deep learning has achieved fruitful results in the field of HSI processing. For example, a 3-D convolution neural network is constructed to extract both spectral and spatial features of the HSI for a better performance of HSI classification [23]; a three-layer convolution neural network is constructed by enlarging the MSI and taking the pan sharpening image as input to obtain a higher resolution MSI [24]; and a recurrent neural network is used to learn the transfer rules for land cover CD [25], and so on.

Due to the instrumental errors of the hyperspectral imager itself and atmospheric scattering during data collection, the collected HSI data contain a lot of noise. If only the spectral information corresponding to a pixel is used when detecting whether a pixel changes, the CD process will be affected by noise and the detection performance will be greatly decreased [26]. Therefore, in addition to deeply exploiting spectral information, some advanced deep learning CD methods usually exploit certain spatial features as an aid to improve the accuracy, that is, "spectral–spatial combination." Spectral–spatial combination is the key of the method for processing and analyzing HSI by fusing spectral and spatial information. These methods have been widely used in the classification of hyperspectral imagery [23].

Based on the above-mentioned problems, this article develops a three directions spectral–spatial convolution neural network (TDSSC) for HSI CD problems. First, the difference map of the bitemporal HSI data is used as input of TDSSC. To make full use of the rich HSI spectral information, the change tensor is then decomposed in three directions to obtain the tensor containing spectral information and the tensor containing both spectral and spatial information, and the spectral and spectral–spatial features are extracted by 1-D and 2-D convolutions, respectively. After that, all the features are fused and binary classifications are made to extract the changing areas according to the classification results.

TDSSC uses the theory of deep learning to process high-dimensional change tensors from different directions. The main advantages are numerous. The convolution network along the spectral direction extracts rich spectral features while reducing the dimensions of the tensor, which greatly reduces the parameters of the entire network and effectively improves the performance of CD. The convolution network along the two spatial directions provides spectral–spatial features from different directions of tensors, exploiting spectral features and spatial features of the cross section as supplements. It realizes the joint exploitation of spatial information and spectral information, improving the CD accuracy and stability. Compared with the 3-D convolutional neural network (3DCNN), TDSSC is more flexible and can exploit information with different settings in different directions. TDSSC can flexibly adjust the configuration of three-directional convolution according to the HSI to suit different complex situations. Experiments on real datasets show that the TDSSC method proposed in this article has better detection results in the task of HSI CD.

The remainder of this article is divided into four sections. Section II reviews the related research on remote sensing image CD, especially hyperspectral CD. Section III elaborates the proposed TDSSC in detail. Section IV describes our experiments and compares and evaluates some existing CD algorithms, and Section V summarizes this article.

II. Related Work

Binary CD is a common type of remote sensing image CD. Its purpose is to classify multitemporal remote sensing images' pixels into the changed and the unchanged. The relevant CD methods are summarized below.

A. Traditional Method

If the spectral information of remote sensing image in two temporals corresponding to one pixel changes greatly, that suggests that this pixel has changed. Therefore, change vector analysis (CVA) [27] is a common method and usually applied for CD. CVA determines whether a pixel changes by calculating its spectral change vector in two temporals and getting its magnitude and direction of change. There have also been many studies on the promotion and improvement of CVA, such as that by Bovolo and Bruzzone [28], who introduced a formal definition framework for CVA methods in polar coordinate systems to solve the unsupervised CD problem.

Due to a large amount of data redundancy in HSI data, it is a natural idea to reduce the dimensionality of the data, and the loss of information caused by this dimensionality reduction should be as small as possible. Principal component analysis (PCA) [29] is a widely used data dimension reduction method, which can map the original features linearly into a specified dimension, cause the mapped features to retain the information of the original features to the maximum extent, and achieve the effect of dimension reduction. Canonical correlation analysis (CCA) [30] in multivariate statistical analysis is also a method of data dimension reduction. CCA transforms two sets of high-dimensional data into two 1-D vectors with the largest correlation coefficient. The multivariate alteration detection (MAD) [31] method is based on CCA. MAD calculates the value of the MAD variable by solving the parameters in the optimization problem to determine whether each pixel has changed. After that, Nielsen [32] proposed an iteratively reweighted multivariate CD method (IR-MAD) based on the MAD. Each pixel is given a weight to participate in the calculation during the iteration. After the iteration is completed, the weight is used as the criterion to determine whether the pixel changes.

There is also a simple supervised classification strategy for CD of remote sensing images. Bovolo *et al.*'s [33] CD framework classifies two temporals remote sensing images pixel by pixel. If a pixel's classification results are different, it can be established that the pixel has changed. Nemmour and Chibani [34] proposed a CD method based on a multisupport vector machine that uses a similar strategy.

It can be seen that traditional CD methods extract the features of spectral change vectors by algebraic operation, image transformation, and statistical analysis of spectral change vectors, which can be easily implemented in low-dimensional space with high accuracy. In high-dimensional space, however, some algebraic processing becomes difficult. For example, in many methods, the inversion of a matrix is often difficult and may cause a loss of precision in high-dimensional situations. Therefore, deep learning has become an important method to solve this problem.

In addition, the methods based on fractional Fourier entropy and fractional Fourier transform provide some interesting ideas for HSI CD without deep learning. Tao *et al.* [35] first proposed the fractional Fourier method to obtain features in an intermediate domain between the original reflectance spectrum and its Fourier transform with complementary strengths by space–frequency representations, which has emerged as a new branch in hyperspectral target anomaly detection.

B. Deep Learning Method

As mentioned in Section I, deep learning is an important method for processing high-dimensional data and has important applications in remote sensing image classification and change detection. Zhao *et al.* [36] used deep learning to extract unsupervised features from the differentiated images, and made some adjustments to the results using supervised preclassification.

As also mentioned in Section I, the process of extracting features using spectral information alone is susceptible to noise, so, many of the existing advanced methods use deep learning to exploit spectral features while also exploiting other features of the HSI for the purpose of improving accuracy. The GETNET framework proposed by Wang *et al.* [37] incorporates the results of linear and nonlinear HSI unmixing into the mixed affinity matrix. The end element abundance of information at the subpixel level is fully utilized, effectively improving the accuracy of hyperspectral CD. Huang *et al.* [38] established the information model called TFS-Cube for the change of the underlying features of HSI, made full use of the change information gained thereby, and used the support tensor machine instead of the back-propagation (BP) network for supervised learning, which improved the performance of the detection of HSI CD. Chen *et al.* [39] proposed a spectral–spatial regularization low-rank sparse decomposition model, LRSDASS, which decomposes the spectral change vectors into low-rank data, abnormal sparse values, and noise in order to extract clean features.

In addition, the exploitation of spatial information has also achieved good results in CD. Ran *et al.* [40] proposed a one-class sparse representation classifier (OCSRC) based on spectral–spatial combination. The Gabor filter, adaptive weighted filter, and cooperative representation filter were extracted from the original HSI by convolution to combine the information of neighboring pixels. Karmon *et al.* proposed a fused spectral–spatial eigenvector and applied it to a CD model based on maximum likelihood correlation coefficient to generate test statistics to describe the change [41]. Therefore, for HSI, in addition to spectral features, using deep learning to exploit spatial and other features is an important research direction to improve the accuracy of CD.

III. Proposed Method

The CD process of the TDSSC we proposed is shown in Fig. 1. For two HSI datasets with different time temporals in the same region, the difference operation is performed on the HSIs to get the hyperspectral change image after removing bands with low signal-to-noise ratio (SNR). Each pixel in the change image corresponds to a spectral change vector. In order to determine whether a pixel has changed, the tensor formed by the hyperspectral change vector of the pixel and its neighboring pixels is used as the input of the model. The model is divided into two parts. The first part uses the input tensor to reduce the dimension through a convolution neural network to obtain a tensor with a lower spectral dimension to use as the input of the second part. In the second part, the reduced dimension tensor block is input into a convolution neural network along two spatial directions to further extract spatial and spectral information, and then, the results of the convolution neural network in two directions and the results of the first part are fused into tensor clusters as the extracted spatial–spectral features. In the third part, after the tensor cluster is pooled, randomly dropped out, and flattened, it is then classified into two categories. The CD result graph is yielded after each pixel is detected.

A. Image Difference

A common practice is image difference operation when showing the change situation of the two temporals HSI data [4]

$$I_D = I_2 - I_1 \tag{1}$$

where I_1 and I_2 are different temporals HSIs, I_D is the hyperspectral change image. In TDSSC, we use the image difference operation with absolute value

$$I_D = |I_2 - I_1| \ . \tag{2}$$

There are two advantages of this image difference method. First, the difference results are all nonnegative numbers, which will bring convenience to the storage and subsequent processing of the results. Second, it focuses on the change magnitude of two spectral vector elements to generate a binary result for change and nonchange.

B. Extract Tensor's Spectral–Spatial Features With Three Directions Convolution Neural Network

Fig. 2 shows the network structure to determine whether a pixel has changed or not. We extract the change tensor of this pixel and its neighbors in I_D to form a change tensor block of $b \times b \times L$, where b is the size of the neighborhood and L is the number of bands. We use a 1-D convolution network to reduce the dimension of the tensor to the specified dimension k and extract the spectral characteristics of the tensor. The reduced-dimension $b \times b \times k$ tensors are input into a 2-D convolution network along two spatial directions to extract spectral–spatial features at different directions. The two features are fused and

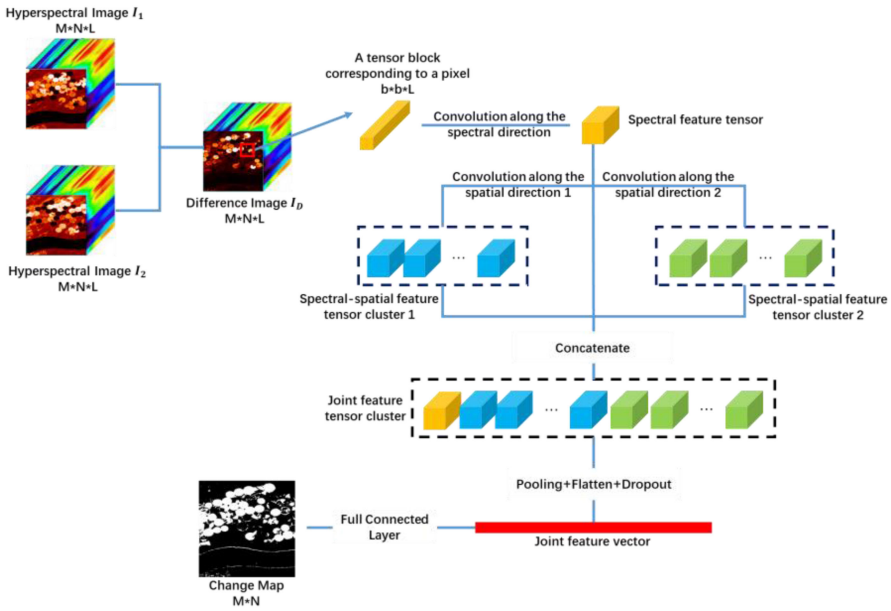

Fig. 1. Overview of CD process of TDSSC.

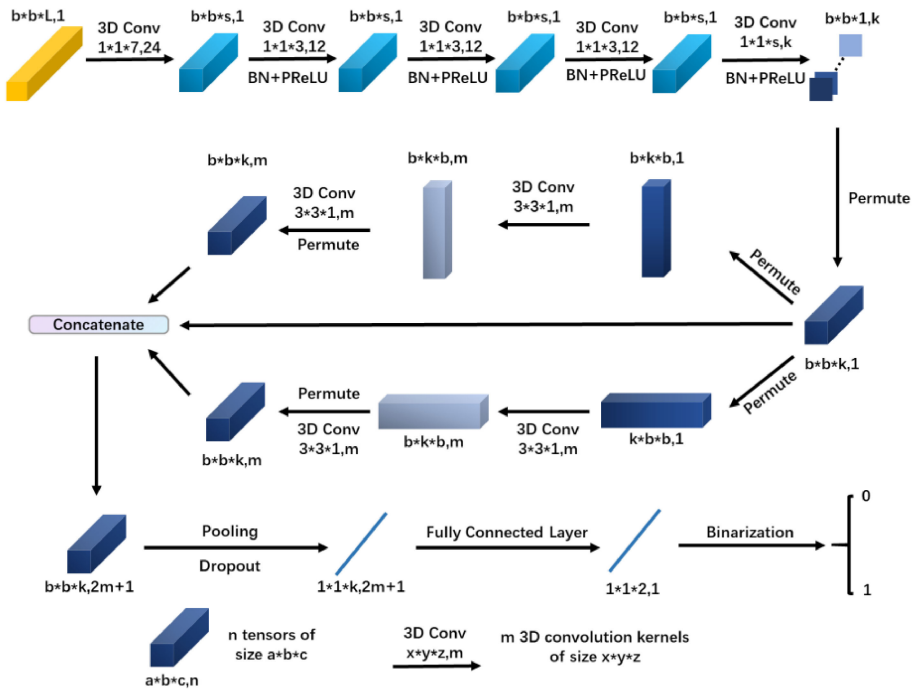

Fig. 2. Structure of the three-directions convolution neural networks for change tensor.

then pooled into the fully connected layer for classification. For convenience, we use 3-D convolution to implement the three directions convolution neural network.

1) Three-Directional Decomposition of Change Tensor: Fig. 3 shows the way of three-directional decomposition of an HSI change tensor. Consider an HSI change tensor with a size of b × b × p, where b is the spatial dimension and p is the spectral dimension. The tensor is decomposed in the spectral direction and two spatial directions as follows—in the spectral direction, the tensor is decomposed into b × b tensors with a size of 1 × 1 × p, which contain the spectral information of the change tensor; in each spatial direction, b tensors are sliced along the corresponding spatial direction, which combine spatial information with spectral information and are rarely explored. The spectral–spatial information obtained from slicing a tensor in two spatial directions, which combines the spectral information with spatial information, is a rarely noticed tensor feature. It is worth noting that although neighboring data are used in

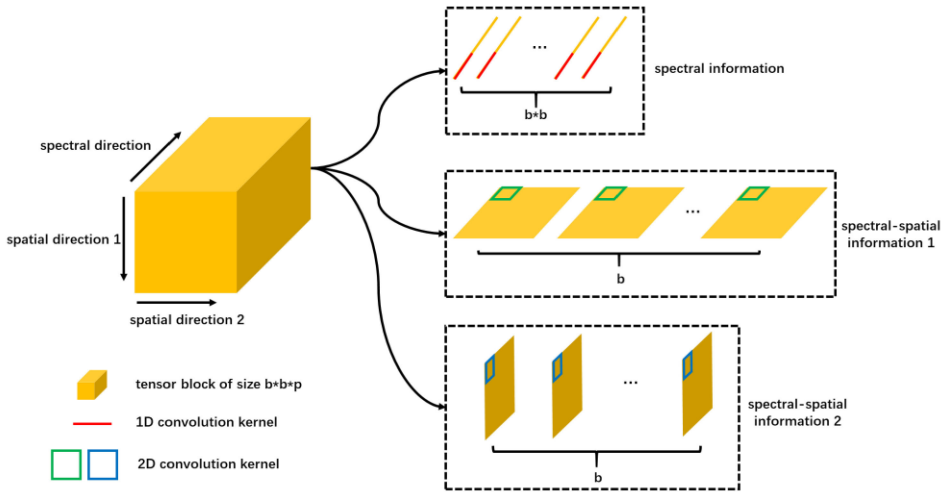

Fig. 3. Way of three-directional decomposition of HSI change tensor.

the spectral direction, we do not use 2-D convolution networks to extract spatial information in the spectral direction. This design is based on our observation that the spatial information extracted by 2-D convolution networks in the spectral direction does not improve the accuracy and may cause some side effects. Compared with HSI, the spatial information along the spectral direction is largely missing from the change image, and there are a large number of scattered areas in the change image, and the characteristics of these scattered areas are often eliminated in the operation of multilayer convolution network, which is reflected in the result of change detection that changes in scatter areas are difficult to detect, resulting in reduced detection accuracy.

2) Extraction of Spectral Features and Tensor Dimension Reduction: The difference of spectral information of a pixel is the main basis for judging whether the pixel has changed. One-dimensional convolution can classify and extract the spectral information of a single pixel [42], so we use a number of 3-D convolution kernels with the size of $1 \times 1 \times s$ to extract the spectral features of the change tensor in the spectral direction. The spectral features of the change tensor can be extracted in the spectral direction by using several 3-D convolution kernels with a size of $1 \times 1 \times s$. At the same time, the convolution of $1 \times 1 \times s$ can reduce the spectral dimension of the tensor block. Each convolution kernel of $1 \times 1 \times s$ represents a dimension reduction method, and the parameters in each convolution kernel are automatically learned by the neural network. Therefore, the convolution neural network of $1 \times 1 \times s$ convolution kernel can extract the spectral features of $b \times b \times L$ tensor and reduce the tensor to $b \times b \times k$, where k is the spectral dimension after dimension reduction. This can save computing and storage resources effectively, and greatly reduce the number of parameters to be learned in the later network, which significantly improves the performance of change detection.

In order to speed up the convergence and reduce the resource consumption of the model, except for the first convolution operation, we carried out batch normalization [43]. Batch normalization can effectively avoid the problem of gradient disappearance and speed up the convergence of the model by forcing the distribution of input values back to the standard normal distribution.

After batch normalization, a nonlinear factor is applied to the convolution method through the PReLU activation function [44]. The expression for the PReLU activation function is as follows:

$$\text{PReLU}\ (x_i) = \begin{cases} x_i \text{ if } x_i > 0 \\ a_i x_i \text{ if } x_i \leq 0 \end{cases} \tag{3}$$

where x_i represents the input of channel i and a_i is a parameter which can be automatically learned from BP network. The updating expression is as follows:

$$\Delta a_i \leftarrow \mu \Delta a_i + \text{lr} \frac{\partial \varepsilon}{\partial a_i} \tag{4}$$

where μ is momentum, ε is objective function, and lr is learning rate. Although the PReLU function introduces new learning parameters in the network based on the ReLU function [45], compared with the speed of model convergence, the cost of new learning parameters can be ignored.

3) Extract Spectral–Spatial Features From Different Directions: After dimensionality reduction, the tensor block contains spectral features, but as mentioned in Section I, only using spectral features for CD is susceptible to noise, and the lack of spatial features mining, both of which make the accuracy of CD difficult to improve. Section I mentions that slicing tensors in spatial direction to combine spatial and spectral information and 2-D convolution is a good way to extract both features [42]. First, transform the reduced dimension $b \times b \times k$ tensor into $b \times k \times b$ and $k \times b \times b$ tensor blocks, and then, the spectral–spatial features of these two tensor blocks are extracted by a spatial convolution neural network composed of a convolution kernel with the size $3 \times 3 \times 1$. Due to the contribution of the two spatial directions' convolution neural networks to the extraction of spectral–spatial features being approximately the same, the structure of the two networks is consistent in principle. After two permuted tensor blocks pass through the convolution neural network, a total of 2m tensors whose sizes are $b \times b \times k$ can be obtained, where m is the number of convolution kernels. By

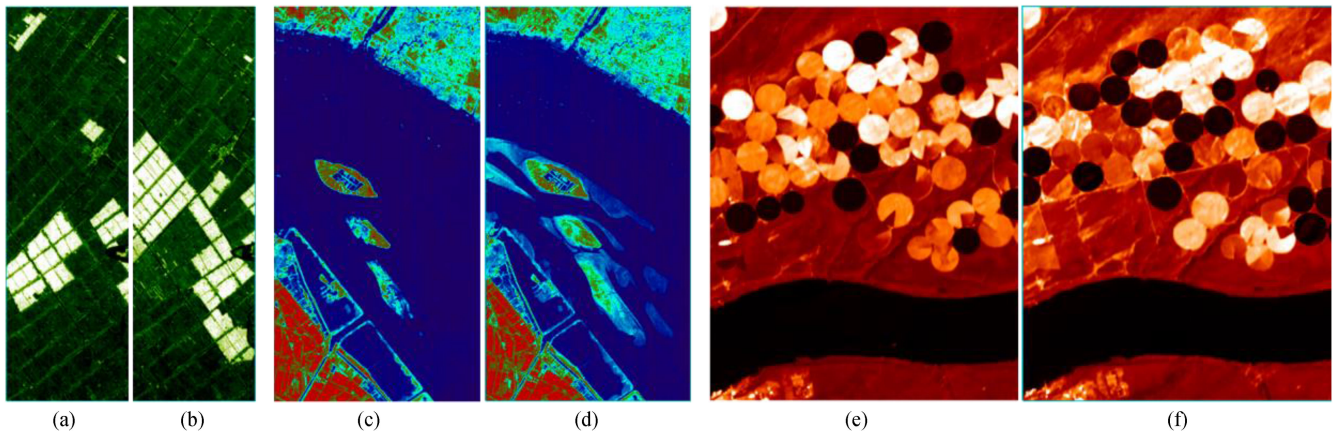

Fig. 4. Datasets in this article. (a) Farmland imagery on May 3, 2006. (b) Farmland imagery on April 23, 2006. (c) River imagery on May 3, 2013. (d) River imagery on December 31, 2013. (e) USA imagery on May 1, 2004. (f) USA imagery on May 8, 2007.

fusing the tensor block with spectral features information from before, we can get $2m + 1$ tensors, whose size is b $\times$ b $\times$ k with spatial features and spectral features for CD. In this part, batch normalization and the PReLU activation function are still used, and its function can be seen in detail in Section I.

The convolution of the two spatial directions combines the information of each band and space. Different convolution kernels are used to mine different spectral–spatial features, which results in high flexibility. The number of convolution kernels and convolution layers can be adjusted freely according to the features of HSI data.

C. CD Based on Fusion Features

The tensor cluster that combines spatial and spectral features is pooled, randomly dropped out, and flattened, then converted into vectors and input the fully connected layer to get the probability that the pixel belongs to the unchanged and changed pixel, and then binarized to determine their change situation. After each pixel completes the CD, it can draw the image of the change area and use the formula to calculate the relevant evaluation parameters to evaluate the CD effect.

Since we treat CD as a binary classification problem, in TDSSC, we use cross entropy loss function to perform a softmax regression.

The details framework of TDSSC is shown in Algorithm 1.

Algorithm 1: Framework of TDSSC for HSI CD.

Input:

1) Two HSIs of the same region at different time temporals with ground truth.
2) The number of training samples N_t, the number of validation samples N_v, the spatial size of input change tensors w, the number of epochs N_e.

Step 1: Achieve the change image of two HSIs by image difference operation.

Step 2: Extract the change tensors separately with the available pixels at the center. The size of the change tensor is w $\times$ w $\times$ L, where L is the number of bands in HSIs.

Step 3: Randomly select N_t tensors as the training set G_{train}, randomly select N_v tensors as the validation set $G_{\text{validation}}$, and the remaining change tensors are set as the testing set G_{test}.

Step 4: Use G_{train}, $G_{\text{validation}}$, and the corresponding label sets L_{train}, $L_{\text{validation}}$ as the input to the network.

Step 5: The gradient descent method is used to optimize iteratively to obtain the optimal model. If the validation loss does not decrease for N_e consecutive epochs, the training is aborted and the last model that reduced the validation loss is set as the optimal model.

Step 6: Put G_{test} into the trained model to predict the change detection results.

Output:

1) Change map
2) OA, Kappa

IV. Experiments

In this section, we will first introduce the HSI datasets used in the experiment, then introduce the evaluation indicators of the selected method, and finally, give the experiment's results and our analysis.

A. Datasets in the Experiments

In the experiment of this article, three groups of HSI data are used, the "Farmland" dataset and the "River" dataset are taken from [37], both of which are collected from Earth Observing-1 (EO-1) Hyperion. The spectral range of EO-1 is 0.4–2.5 μm, the spectral resolution is about 10 nm, and the spatial resolution is about 30 m, including 242 bands in total. However, due to the impact of internal and external noise during the imaging process, some spectral information of the band will be destroyed. The

"USA" dataset is from [46], and its data are also collected from Hyperion sensor.

The first dataset "Farmland" is an HSI of a farmland near Yancheng City, Jiangsu Province, on May 3, 2006 [see Fig. 4(a)] and April 23, 2007 [see Fig. 4(b)] with a size of 450 × 140 pixels. After noise elimination, 155 bands remain. Training effect is closely related to the number of samples used for training. In order to facilitate the comparison and evaluation of the model, we select about 20.95% of the total pixels as the training data according to the training sample setting method in [37], including 4400 changed pixels and 8800 unchanged pixels. As mentioned in [37], the ratio of changed pixels in the Farmland dataset is higher than those in other experimental datasets, so we choose more training samples.

The second dataset "River," a dataset and ground truth map, is also established by [37]. The dataset is selected from two HSIs of a river in Jiangsu Province on May 3, 2013 [see Fig. 4(c)] and December 31, 2013 [see Fig. 4(d)], with a size of 463 × 241 pixels. From 242 bands, 198 bands with high signal-to-noise ratio (SNR) are selected. In order to facilitate comparison and evaluation, about 3.37% pixels are selected as training data, including 1250 changed pixels and 2500 unchanged pixels.

The third dataset "USA" shows the situation of an irrigated farmland in the USA on May 1, 2004 [see Fig. 4(e)] and May 8, 2007 [see Fig. 4(f)]. With the size of 307 × 241 pixels, 154 bands with high SNR are selected. The land cover types include soil, irrigation area, river, building, cultivated land type, and grassland. Referring to the setting in [46], we select about 9.77% of pixels as training data, including 3313 changed pixels and 3919 unchanged pixels.

B. Algorithm Evaluation Measures

The method to evaluate the effect of a CD algorithm is to compare the predicted results of the model with the ground truth map and calculate the accuracy of the algorithm. We use the two indexes of overall accuracy (OA) and the kappa coefficient to evaluate the CD effect of the algorithm. In order to calculate OA and kappa values, we need to count the prediction of each pixel of the model—number of changed pixels correctly classified as TP (true positive); number of unchanged pixels correctly classified as TN (true negative); number of changed pixels incorrectly classified as FP (false positive); number of unchanged pixels incorrectly classified as FN (false negative). Let K equal the total number of all the pixels, then we have

$$\mathrm{K} = \mathrm{TP} + \mathrm{TN} + \mathrm{FP} + \mathrm{FN}. \tag{5}$$

OA is used to measure the correct classification pixel proportion of the algorithm. The formula is

$$\mathrm{OA} = \frac{\mathrm{TP} + \mathrm{TN}}{\mathrm{K}}. \tag{6}$$

Kappa coefficient measures the consistency between the prediction results of the algorithm and the ground truth map, and the formula is as follows:

$$\mathrm{Kappa} = \frac{\mathrm{OA} - \mathrm{p_e}}{1 - \mathrm{p_e}} \tag{7}$$

where the formula of $\mathrm{p_e}$ is

$$\mathrm{p_e} = \frac{(\mathrm{TP} + \mathrm{FP})(\mathrm{TP} + \mathrm{FN})}{\mathrm{K^2}} + \frac{(\mathrm{TN} + \mathrm{FP})(\mathrm{TN} + \mathrm{FN})}{\mathrm{K^2}}. \tag{8}$$

C. Experiment Results and Analysis

In this article, the change of HSI is pixel-level change. We improve the accuracy of CD by fusing the extracted change tensor with the combined spectral and spectral–spatial features obtained along the spectral direction and two spatial directions, respectively. We compare TDSSC with other common CD methods, including CVA [27], PCA-CVA [29], support vector machine (SVM) [34], patch-based CNN, and GETNET [37] to illustrate the effectiveness and advantages of TDSSC. We choose these algorithms because they cover the techniques and strategies commonly used in CD, such as algebraic operations, image transformation, and deep learning.

We have implemented TDSSC using Keras with Tensorflow as backend. TDSSC does not need the model of pretraining. The training batch size is 512, the optimizer selects Adam, and its parameter is the default parameter. In each convolution operation, we introduce L2 regularization to avoid overfitting as much as possible, in which the regularization parameter $\lambda = 0.0001$. In addition, early stopping is introduced in the model to reduce overfitting. We determine if training needs to be aborted by monitoring the accuracy of the model on the validation set. Considering that there are some random factors in the algorithm of deep learning, such as a dropout layer, in order to evaluate the methods of deep learning objectively, each deep learning method runs four times on each dataset, with its average value and standard deviation as the measurement standard. In addition, to explore the role of spectral–spatial features in TDSSC, we remove the convolution neural networks of two spatial directions in TDSSC. That is, directly detect change after dimensionality reduction and extraction of spectral features. We make it another method in our experiment.

In TDSSC, the spatial dimension b of the extracted change tensor and the spectral dimension k after dimension reduction are two important parameters. The reasonable selection of the values of the parameters b and k will help to fully extract the spectral features and lay the foundation for the later application of spatial directions convolution neural network to mine the spectral–spatial features. We traverse the combination of b and k in a reasonable range for TDSSC (without spatial convolution). For each dataset, we choose the combination that produces the largest OA as the combination of b and k corresponding to the dataset. Considering the performance and stability of TDSSC, in this experiment, the value of b is chosen from set $\{3, 5, 7, 9\}$, and the value of k is chosen from the following set: $\{\mathrm{k} | 15 \leq \mathrm{k} \leq 120, \mathrm{k} = 5\mathrm{p}, \mathrm{p} \in \mathrm{N}\}$.

1) Experiment on the Farmland Dataset: The Farmland dataset mainly describes the change of cultivated land. First, b and k which are suitable for the Farmland dataset are selected according to the CD results of TDSSC (without spatial convolution). Fig. 5 shows the CD OA of different

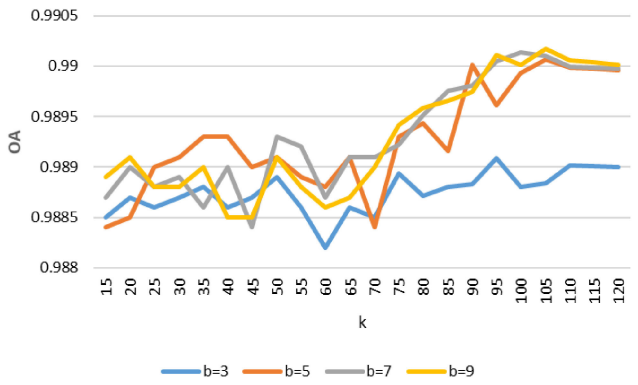

Fig. 5. CD OA of different parameter combinations on Farmland.

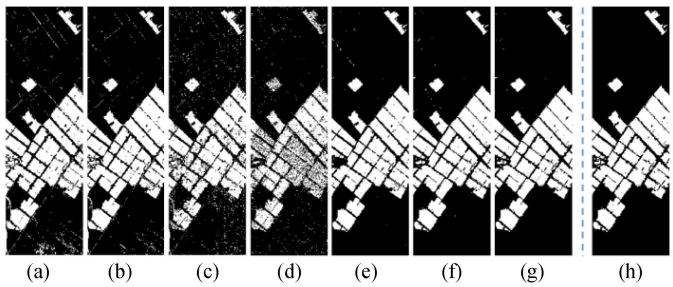

Fig. 6. CD result of different methods on Farmland dataset. (a) CVA. (b) PCA-CVA. (c) SVM. (d) CNN. (e) GETNET. (f) TDSSC (without spatial convolution). (g) TDSSC. (h) Ground truth.

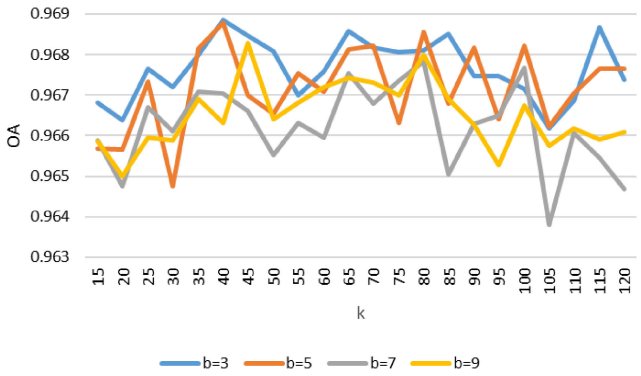

Fig. 7. CD OA of different parameter combinations on River.

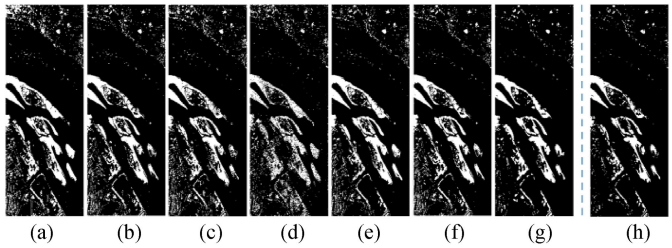

Fig. 8. CD result of different methods on River dataset. (a) CVA. (b) PCA-CVA. (c) SVM. (d) CNN. (e) GETNET. (f) TDSSC (without spatial convolution). (g) TDSSC. (h) Ground truth.

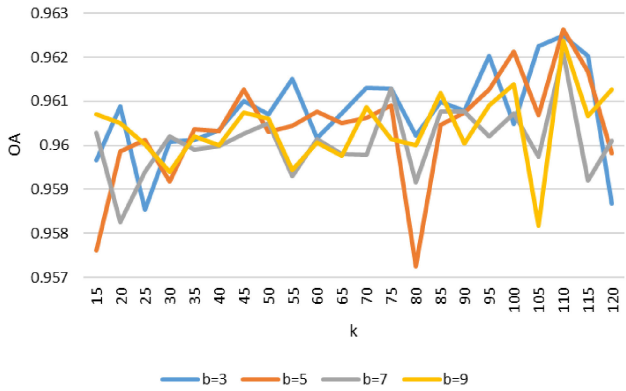

Fig. 9. CD OA of different parameter combinations in USA.

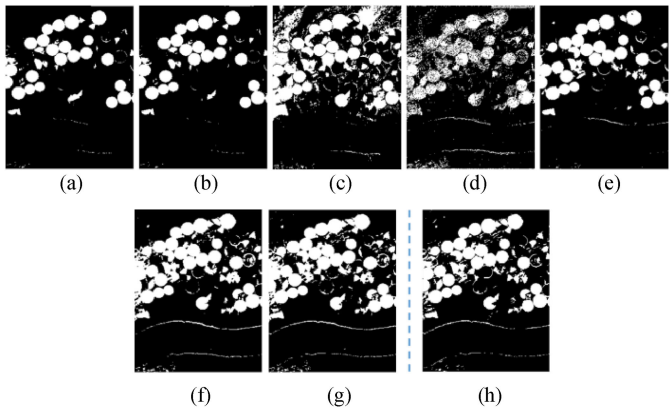

Fig. 10. CD result of different methods in the USA dataset. (a) CVA. (b) PCA-CVA. (c) SVM. (d) CNN. (e) GETNET. (f) TDSSC (without spatial convolution). (g) TDSSC. (h) Ground truth.

parameter combinations. In Farmland's experiment, we choose the parameter combination of b = 9, k = 105.

Fig. 6(a)–(g) shows the CD results of each experimental method on Farmland. From the ground truth Fig. 6(h), it can be seen that most of the changes in the Farmland dataset are concentrated and have regular shapes, and the pixel proportion of the changed and unchanged pixels is also relatively balanced. Therefore, both the traditional CD method and the CD method based on deep learning have a good performance in this dataset. In terms of the OA and kappa coefficient, TDSSC significantly improves the accuracy of CD. In the method of using a neural network, the lack of spatial information mining by CNN leads the classification effect to be easily affected by much HSI redundancy and noise. GETNET and TDSSC can better extract the features of HSI. Compared with GETNET, our method can more fully extract the spectral and spatial features. In this experiment, we notice that the spectral–spatial features used in TDSSC can improve the accuracy of CD in a limited way, which is related to the change of the dataset itself. The change of Farmland is more concentrated, the extracted change tensor contains the information of neighboring pixels, and the number of training samples is sufficient. The convolution neural network in the spectral direction can provide enough change features, so the increase of spectral–spatial features can bring mostly

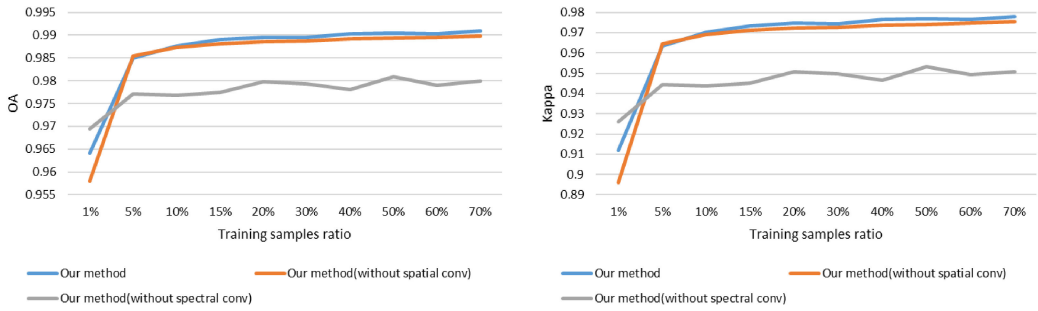

Fig. 11. OA and kappa coefficient line graphs of TDSSC (without spatial convolution), TDSSC (without spectral convolution), and TDSSC on Farmland dataset.

TABLE I
OA AND KAPPA COEFFICIENTS OF TDSSC AND OTHER ADVANCED CD METHODS ON THREE DATASETS

Method	Index	Experiment Data sets		
		Farmland	River	USA
CVA	OA	0.9523	0.9267	0.9200
	Kappa	0.8855	0.6575	0.7410
PCA-CVA	OA	0.9668	0.9516	0.9153
	Kappa	0.9202	0.7477	0.7225
SVM	OA	0.9376	0.9424	0.8810
	Kappa	0.8483	0.7066	0.6848
CNN	OA	0.9185	0.9139	0.8902
	Kappa	0.7949	0.5585	0.6699
GETNET	OA	0.9753±0.0003	0.9499±0.0054	0.9430±0.0010
	Kappa	0.9394±0.0008	0.7472±0.0215	0.8249±0.0030
TDSSC (without spatial convolution)	OA	0.9900±0.0004	0.9708±0.0019	0.9615±0.0008
	Kappa	0.9751±0.0010	0.8168±0.0087	0.8842±0.0020
TDSSC	OA	**0.9904±0.0004**	**0.9737±0.0011**	**0.9631±0.0007**
	Kappa	**0.9759±0.0009**	**0.8310±0.0058**	**0.8890±0.0018**

confirmatory information, which is helpful for the improvement of robustness and kappa value.

2) Experiment on the River Dataset: Some solid materials in the river and the changes of topography are the main changes of the River dataset. Similarly, b and k, which are suitable for River dataset, are selected according to the CD results of TDSSC (without spatial convolution). Fig. 7 shows the CD OA of different parameter combinations. In River's experiment, we choose the parameter combination of b = 3, k = 115.

Fig. 8(a)–(g) shows the CD results of each experimental method on River. Compared with the Farmland dataset, the River dataset is much more difficult. First of all, the proportion of the changed to unchanged pixels is quite different, less than 1:10. Second, from the ground truth map Fig. 8(h), it can be seen that a large number of changes are scattered, and the multilayer convolution operation may cause the features of these changed pixels to be eliminated. In addition, the dataset is complex and diverse, and the number of selected training samples is small, which necessitates a higher level of deep learning algorithm requirement. From the experimental results, the kappa coefficient is generally reduced due to the great difference between the positive and negative samples in the dataset. However, TDSSC still has the best results, and the spectral–spatial features greatly improve the evaluation index, which shows that the spectral–spatial features make up for the weakness of the spectral features vulnerable to noise, and improve the consistency of CD.

3) Experiment on USA Dataset: The USA dataset mainly describes the changes of some land in irrigated farmland. Parameters b and k, which are suitable for the USA dataset, are selected according to the CD results of TDSSC (without spatial convolution). Fig. 9 shows the CD OA of different parameter combinations. In Farmland's experiment, we choose the parameter combination of b = 3, k = 110.

Fig. 10(a)–(g) shows the CD results of each experimental method on the USA dataset. From the ground truth map Fig. 10(h), the change of the dataset is more complex, the shape of the change area is mainly circular, and it contains a large number of irregular areas, curves, and scattered points, which is a relatively comprehensive and quite difficult CD task. From the experimental results, the scattered area above and the river edge below are the difficulties that affect the change accuracy. The traditional CD method is not sensitive to irregular areas, curves, and scattered points, which is still the main reason for its low accuracy. There are some problems in the processing of the

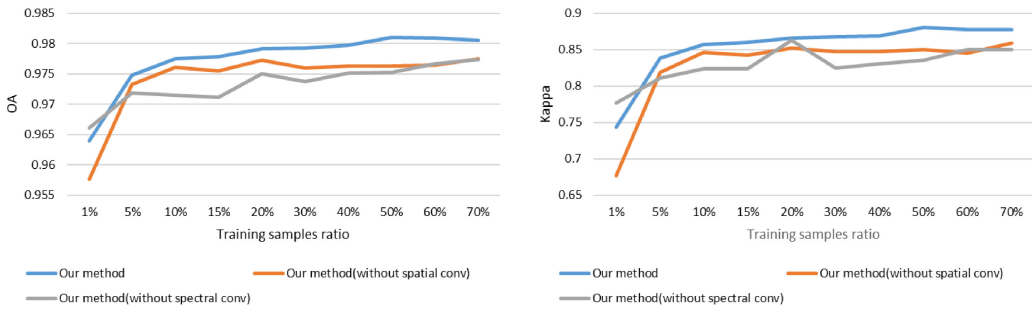

Fig. 12. OA and kappa coefficient line graphs of TDSSC (without spatial convolution), TDSSC (without spectral convolution), and TDSSC on River dataset.

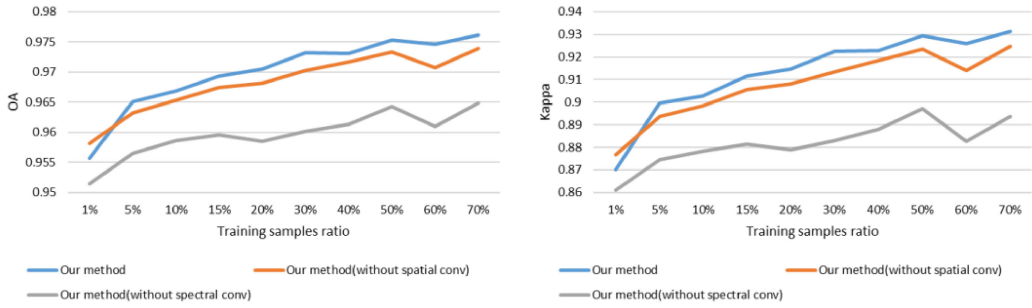

Fig. 13. OA and kappa coefficient line graphs of TDSSC (without spatial convolution), TDSSC (without spectral convolution), and TDSSC on USA dataset.

river edge with GETNET. TDSSC can deal with the above two difficulties well while still achieving the best results in accuracy and consistency. This proves once again that TDSSC can extract the features of change tensor more fully.

The experimental results of different methods in the three groups of experimental data are shown in Table I.

4) Ablation Experiments: We evaluated the role of various components of TDSSC by ablation experiments. TDSSC contains one convolution network along the spectral direction and two convolution networks along the spatial direction. Considering that the two convolution networks in the spectral direction have the same status, we will consider them as part of the discussion. To investigate the performance of each part in different sample sizes, we compared the results of TDSSC (without spatial directional convolution), TDSSC (without spectral directional convolution), and TDSSC in different training sample sizes. We calculated the ratio of the number of pixels in each dataset, and selected the same proportion of training samples. In the same proportion of training samples, the training samples of the two methods are the same. The proportion of the selected samples is divided into the following ten levels: 1%, 5%, 10%, 15%, 20%, 30%, 40%, 50%, 60%, and 70%, covering all scenarios in a range of training samples. In the case of fewer samples, the number of parameter updates may be too low if the batch value is too large, so the batch setting of the three methods in this experiment is 128, and the rest of the settings are unchanged.

Figs. 11–13 show the effect of these three methods on the three groups of experimental data. From the results, the fusion of spectral–spatial features can increase OA by 0.1%–0.3% on average, and kappa coefficient by 0.4%–1.5%. This shows that TDSSC can adapt to various training samples. These improvements are most obvious on the River dataset and less so on the Farmland dataset, which has a lot to do with the dataset itself. If a dataset is the same as the Farmland in terms of changing area rules, few scattered areas, and small data noise, then the spectral features are almost enough to provide all the changing features, and the spectral–spatial features are in more of a confirmatory role; conversely, in the datasets with complex and diverse changes, many scattered change areas, and large data noise, the features of spectral–spatial combination can supplement and repair the missing and disturbed features in the spectral features.

It is interesting to note that, although the spectral–spatial features learned by convolutions in two spatial directions are ancillary, in ablation experiments, it can be seen that only the spectral–spatial features are better than the complete TDSSC in only a very few samples, indicating that the spatial joint features are less susceptible to noise.

V. Conclusion

In this article, we propose a three-directions spectral–spatial convolution neural network called TDSSC. We decompose the change tensor along the spectral direction and two spatial directions, respectively, and obtain the tensor containing spectral information and the slice tensor containing the combination of spectral and spatial information. TDSSC uses a 1-D convolution network to extract the spectral features of change tensors, while reducing the dimension of change tensors to the specified space, which makes the whole network lightweight and significantly improves the speed of CD. 2-D convolution extracts the spectral–spatial features of change tensors after dimension

reduction, which combines spatial and spectral information to minimize the impact of noise. TDSSC can extract the features of a hyperspectral change tensor by building a convolution neural network of three directions, improve the accuracy and consistency of CD, and at the same time, it is more flexible than other methods. According to the change features of different datasets, the network structure can be adjusted appropriately to obtain better results. Experiments are carried out on real HSI datasets, and the results are compared with those of several advanced CD methods. The OA and kappa value of the detection results of the method in this article have achieved the best detection results on three datasets. The results show that the proposed method can effectively improve the accuracy of hyperspectral CD because it deeply explores the difference image from spectral and spatial directions from different angles and fully excavates the depth of "spectral–spatial" features.

In our future work, the application of the superpixel in TDSSC may be explored. Superpixels is anticipated to perform better in the task of extracting spatial information from change images than the fixed windows used in traditional convolutional networks.

REFERENCES

[1] J. Yan *et al.*, "A time-series classification approach based on change detection for rapid land cover mapping," *ISPRS J. Photogramm. Remote Sens.*, vol. 158, pp. 249–262, 2019.

[2] V. Ferraris *et al.*, "Coupled dictionary learning for unsupervised change detection between multimodal remote sensing images," *Comput. Vis. Image Understanding*, vol. 189, 2019, Art. no. 102817.

[3] A. Benedetti, M. Picchiani, and F. Del Frate, "Sentinel-1 and Sentinel-2 data fusion for urban change detection," in *Proc. IEEE Int. Geosci. Remote Sens. Symp.*, 2018, pp. 1962–1965.

[4] S. Liu, D. Marinelli, L. Bruzzone, and F. Bovolo, "A review of change detection in multitemporal hyperspectral images: Current techniques, applications, and challenges," *IEEE Geosci. Remote Sens. Mag.*, vol. 7, no. 2, pp. 140–158, Jun. 2019.

[5] B. Tu *et al.*, "Hyperspectral anomaly detection via density peak clustering," *Pattern Recognit. Lett.*, vol. 129, pp. 144–149, 2020.

[6] W. Xie *et al.*, "Spectral constraint adversarial autoencoders approach to feature representation in hyperspectral anomaly detection," *Neural Netw.*, vol. 119, pp. 222–234, 2019.

[7] N. Acito, M. Diani, G. Corsini, and S. Resta, "Introductory view of anomalous change detection in hyperspectral images within a theoretical Gaussian framework," *IEEE Aerosp. Electron. Syst. Mag.*, vol. 32, no. 7, pp. 2–27, Jul. 2017.

[8] X. Yao and C. Zhao, "Hyperspectral anomaly detection based on the bilateral filter," *Infrared Phys. Technol.*, vol. 92, pp. 144–153, 2018.

[9] S. Song *et al.*, "Hyperspectral anomaly detection based on anomalous component extraction framework," *Infrared Phys. Technol.*, vol. 96, pp. 340–350, 2019.

[10] C. Mu *et al.*, "Accelerated genetic algorithm based on search-space decomposition for change detection in remote sensing images," *Appl. Soft Comput.*, vol. 84, 2019, Art. no. 105727.

[11] A. Ertürk, M. Iordache, and A. Plaza, "Hyperspectral change detection by sparse unmixing with dictionary pruning," in *Proc. 7th Workshop Hyperspectral Image Signal Process., Evol. Remote Sens.*, 2015, pp. 1–4.

[12] A. Ertürk, M. Iordache, and A. Plaza, "Sparse unmixing-based change detection for multitemporal hyperspectral images," *IEEE J. Sel. Topics Appl. Earth Observ. Remote Sens.*, vol. 9, no. 2, pp. 708–719, Feb. 2016.

[13] C. P. Dalmiya, N. Santhi, and B. Sathyabama, "A novel feature descriptor for automatic change detection in remote sensing images," *Egyptian J. Remote Sens. Space Sci.*, vol. 22, no. 2, pp. 183–192, 2019.

[14] P. Zhang *et al.*, "Change detection based on deep feature representation and mapping transformation for multi-spatial-resolution remote sensing images," *ISPRS J. Photogramm. Remote Sens.*, vol. 116, pp. 24–41, 2016.

[15] Z. Chen and W. Bin, "Spectrally-spatially regularized low-rank and sparse decomposition: A novel method for change detection in multitemporal hyperspectral images," *Remote Sens.*, vol. 9, no. 10, 2017, Art. no. 1044.

[16] C. Wu, L. Zhang, and L. Zhang, "A scene change detection framework for multi-temporal very high resolution remote sensing images," *Signal Process.*, vol. 124, pp. 184–197, 2016.

[17] J. Zhao, J. Yang, Z. Lu, P. Li, and W. Liu, "Change detection based on similarity measure and joint classification for polarimetric SAR images," in *Proc. IEEE Int. Geosci. Remote Sens. Symp.*, Fort Worth, TX, USA, 2017, pp. 1896–1899.

[18] S. Henrot, J. Chanussot, and C. Jutten, "Dynamical spectral unmixing of multitemporal hyperspectral images," *IEEE Trans. Image Process.*, vol. 25, no. 7, pp. 3219–3232, Jul. 2016.

[19] L. Lu *et al.*, "Assessment of urban environmental change using multisource remote sensing time series (2000–2016): A comparative analysis in selected megacities in Eurasia," *Sci. Total Environ.*, vol. 684, pp. 567–577, 2019.

[20] G. Tong *et al.*, "Review of remote sensing image change detection," *J. Image Graph.*, vol. 20, no. 12, pp. 1561–1571, 2015.

[21] L. Bruzzone, S. Liu, F. Bovolo, and P. Du, "Change detection in multitemporal hyperspectral images," in *Multitemporal Remote Sensing: Methods and Applications*, Y. Ban, Ed. New York, NY, USA: Springer-Verlag, 2016, pp. 63–88.

[22] S. Liu, Q. Du, X. Tong, A. Samat, H. Pan, and X. Ma, "Band selection-based dimensionality reduction for change detection in multi-temporal hyperspectral images," *Remote Sens.*, vol. 9, no. 10, pp. 1–23, 2017.

[23] Y. Chen, H. Jiang, C. Li, X. Jia, and P. Ghamisi, "Deep feature extraction and classification of hyperspectral images based on convolutional neural networks," in *IEEE Trans. Geosci. Remote Sens.*, vol. 54, no. 10, pp. 6232–6251, Oct. 2016.

[24] M. Giuseppe *et al.*, "Pansharpening by convolutional neural networks," *Remote Sens.*, vol. 8, no. 7, 2016, Art. no. 594.

[25] H. Lyu, H. Lu, and L. Mou, "Learning a transferable change rule from a recurrent neural network for land cover change detection," *Remote Sens.*, vol. 8, no. 6, 2016, Art. no. 506.

[26] J. Li, J. M. Bioucas-Dias, and A. Plaza, "Exploiting spatial information in semi-supervised hyperspectral image segmentation," in *Proc. 2nd Workshop Hyperspectral Image Signal Process., Evol. Remote Sens.*, 2010, pp. 1–4.

[27] W. A. Malila, "Change vector analysis: An approach for detecting forest changes with Landsat," in *Proc. LARS Symp.*, 1980, pp. 326–335.

[28] F. Bovolo and L. Bruzzone, "A theoretical framework for unsupervised change detection based on change vector analysis in the polar domain," *IEEE Trans. Geosci. Remote Sens.*, vol. 45, no. 1, pp. 218–236, Jan. 2007.

[29] H. Zhang, M. Gong, P. Zhang, L. Su, and J. Shi, "Feature-level change detection using deep representation and feature change analysis for multispectral imagery," *IEEE Geosci. Remote Sens. Lett.*, vol. 13, no. 11, pp. 1666–1670, Nov. 2016.

[30] D. R. Hardoon, S. Szedmak, and J. Shawe-Taylor, "Canonical correlation analysis: An overview with application to learning methods," *Neural Comput.*, vol. 16, no. 12, pp. 2639–2664, Dec. 2004.

[31] A. A. Nielsen, K. Conradsen, and J. J. Simpson, "Multivariate alteration detection (MAD) and MAF postprocessing in multispectral, bitemporal image data: New approaches to change detection studies," *Remote Sens. Environ.*, vol. 64, no. 1, pp. 1–19, 1998.

[32] A. A. Nielsen, "The regularized iteratively reweighted MAD method for change detection in multi- and hyperspectral data," *IEEE Trans. Image Process.*, vol. 16, no. 2, pp. 463–478, Feb. 2007.

[33] F. Bovolo, S. Marchesi, and L. Bruzzone, "A framework for automatic and unsupervised detection of multiple changes in multitemporal images," *IEEE Trans. Geosci. Remote Sens.*, vol. 50, no. 6, pp. 2196–2212, Jun. 2012.

[34] H. Nemmour and Y. Chibani, "Vector machines for land cover change detection: An application for mapping urban extensions," *ISPRS J. Photogramm. Remote Sens.*, vol. 61, no. 2, pp. 125–133, 2006.

[35] R. Tao, X. Zhao, W. Li, H. Li, and Q. Du, "Hyperspectral anomaly detection by fractional Fourier entropy," *IEEE J. Sel. Topics Appl. Earth Observ. Remote Sens.*, vol. 12, no. 12, pp. 4920–4929, Dec. 2019.

[36] J. Zhao, M. Gong, J. Liu, and L. Jiao, "Deep learning to classify difference image for image change detection," in *Proc. Int. Joint Conf. Neural Netw.*, Jul. 2014, pp. 411–417.

[37] Q. Wang, Z. Yuan, Q. Du, and X. Li, "GETNET: A general end-to-end 2-D CNN framework for hyperspectral image change detection," *IEEE Trans. Geosci. Remote Sens.*, vol. 57, no. 1, pp. 3–13, Jan. 2019.

[38] F. Huang, Y. Yu, and T. Feng, "Hyperspectral remote sensing image change detection based on tensor and deep learning," *J. Vis. Commun. Image Representation*, vol. 58, pp. 233–244, 2019.
[39] Z. Chen, M. Sohail, and B. Wang, "Low-rank matrix decomposition with a spectral-spatial regularization for change detection in hyperspectral imagery," in *Proc. Int. Workshop Remote Sens. Intell. Process.*, 2017, pp. 1–3.
[40] Q. Ran, S. Zhao, and W. Li, "Change detection combining spatial-spectral features and sparse representation classifier," in *Proc. 5th Int. Workshop Earth Observ. Remote Sens. Appl.*, 2018, pp. 1–4.
[41] K. Vongsy and M. J. Mendenhall, "Integrating spatial & spectral information for change detection in hyperspectral imagery," in *Proc. 8th Workshop Hyperspectral Image Signal Process., Evol. Remote Sens.*, Los Angeles, CA, USA, 2016, pp. 1–5.
[42] L. Chen, Z. Wei, and Y. Xu, "A lightweight spectral–spatial feature extraction and fusion network for hyperspectral image classification," *Remote Sens.*, vol. 12, no. 9, Jan. 2020, Art. no. 1395.
[43] S. Ioffe and C. Szegedy, "Batch normalization: Accelerating deep network training by reducing internal covariate shift," in *Proc. 32nd Int. Conf. Mach. Learn.*, Lile, France, Jul. 2015, pp. 1–9.
[44] K. He, X. Zhang, S. Ren, and J. Sun, "Delving deep into rectifiers: Surpassing human-level performance on ImageNet classification," in *Proc. IEEE Int. Conf. Comput. Vis.*, Santiago, Chile, 2015, pp. 1026–1034.
[45] A. Krizhevsky, I. Sutskever, and G. Hinton, "ImageNet classification with deep convolutional neural networks," in *Proc. 26th Annu. Conf. Neural Inf. Process. Syst.*, Lake Tahoe, NV, USA, Dec. 2012, pp. 1097–1105.
[46] H. Mahdi and S. S. Teymoor, "Hyperspectral change detection: An experimental comparative study," *Int. J. Remote Sens.*, vol. 39, pp. 1–55, 2018.

Tianming Zhan received the B.S. and M.S. degrees from the School of Math and Statistics, Nanjing University of Information Science and Technology, Nanjing, China, in 2006 and 2009, respectively, and the Ph.D. degree from the School of Computer Science and Engineering, Nanjing University of Science and Technology, in 2013.

He is currently an Associate Professor with the School of Information Engineering, Nanjing Audit University, Nanjing, China. His research interests include hyperspectral image processing, machine learning, and data analysis.

Bo Song received the B.S. degree in information management and information system, in 2019 from Nanjing Audit University, Nanjing, China, where he is currently working toward the M.S. degree in computer science and technology.

His research interests include hyperspectral image processing.

Le Sun received the B.S. degree from the School of Science, Nanjing University of Science and Technology (NUST), Nanjing, China, in 2009, and the Ph.D. degree from the School of Computer Science and Engineering, NUST, in 2014.

He is currently an Associate Professor with the School of Computer and Software, Nanjing University of Information Science and Technology, Nanjing, China. His research interests include hyperspectral image processing, sparse representation, and compressive sensing.

Xiuping Jia (Senior Member, IEEE) received the B.Eng. degree from the Beijing University of Posts and Telecommunications, Beijing, China, in 1982, and the Ph.D. degree in electrical engineering from the University of New South Wales, Canberra, ACT, Australia, in 1996.

Since 1988, she has been with the School of Engineering and Information Technology, University of New South Wales, where she is an Associate Professor. She has authored or coauthored more than 200 publications, including more than 100 articles in leading technical journals and has coauthored the remote sensing textbook titled *Remote Sensing Digital Image Analysis* (Springer-Verlag, 3rd ed., 1999 and 4th ed., 2006). Her research interests include remote sensing, machine learning, and spatial data analysis.

Dr. Jia is a Subject Editor for the *Journal of Soils and Sediments* during recent years and has been an Associate Editor for the IEEE TRANSACTIONS ON GEOSCIENCE AND REMOTE SENSING, since 2005.

Minghua Wan received the B.S. degree in automated institute from the Nanchang University of Aviation, Nanchang, China, in 2003, and the M.S. and Ph.D. degrees in pattern recognition and intelligence systems from the Nanjing University of Science and Technology (NUST), Nanjing, China, in 2007 and 2011, respectively.

He is currently an Associate Professor with Nanjing Audit University, Nanjing, China. He has authored more than 20 scientific papers in pattern recognition and computer vision. His current research interests include face recognition and reduction, and image processing.

Guowei Yang was born in Zhangshu, China, in 1964. He received the B.S. and M.S. degrees from the Department of Mathematics, Jiangxi Normal University, Nanchang, China, in 1985 and 1988, respectively, and the Ph.D. degree from the School of Information Engineering, Beijing University of Science and Technology, Beijing, China, in 2004.

From 2008 to 2009, he was an Advanced Visiting Scholar with the University of Illinois, IL, USA. He is currently a Professor with the School of Information Engineering, Nanjing Audit University, Nanjing, China. He is also a Director of the Artificial Intelligence Society, Vice Director of Extension Engineering of Specialized Committee, China Society of Artificial Intelligence. His research interests include extenics and big data processing.

Zebin Wu (Senior Member, IEEE) received the B.Sc. and Ph.D. degrees in computer science and technology from the Nanjing University of Science and Technology, Nanjing, China, in 2003 and 2007, respectively.

He is currently a Professor with the School of Computer Science and Engineering, Nanjing University of Science and Technology. His research interests include hyperspectral image processing, parallel computing, and remotely sensed big data processing.